Vapor-Sensitive Bragg Mirrors and Optical Isotherms from Mesoporous Nanoparticle Suspensions

Johannes Kobler,[†] Bettina V. Lotsch,[‡] Geoffrey A. Ozin,[‡] and Thomas Bein[†,*]

[†]Department of Chemistry and Biochemistry and Center for NanoScience (CeNS), University of Munich, Butenandtstr. 5-13 (E), D-81377 Munich, Germany, and [‡]Materials Chemistry Research Group, Center for Inorganic and Polymeric Nanomaterials, Lash Miller Chemical Laboratories, Department of Chemistry, University of Toronto, 80 St. George Street, Toronto, Ontario, M5S 3H6, Canada

ABSTRACT The preparation of wavelength-specific Bragg mirrors was realized by an effective and reproducible spin-coating approach using colloidal suspensions of functionalized mesoporous silica nanoparticles and titania sols. Due to the small particle size and the resulting low surface roughness, the formation of multilayers was possible without transmitting defects on the surface with every following coating step. The Bragg reflectors show sensitivity toward specific relative pressures of organic vapors such as toluene, giving rise to optically encoded adsorption properties as a function of solvent pressure and, thus, to optical adsorption isotherms.

KEYWORDS: vapor sensor · porous films · Bragg reflector · nanoparticles · ellipsometry · optical isotherm

Bragg reflectors are multilayer structures composed of alternating layers of two dielectric materials with different refractive indices (*n*). For ideal reflectors, all layers exhibit an optical thickness of $\lambda/4$. The efficiency increases with the number of layer pairs and the contrast of the refractive indices of the low and highly refracting materials.[1,2]

Bragg reflectors are also widespread in nature, for example, in butterfly wings or iridescent elytra of beetles, where chitin layers alternate with different refractive index layers in order to control the apparent color in a wide variety of animals.[3] In the laboratory, these special thin films can be prepared, for example, by alternation of low refractive SiO_2 with highly refractive TiO_2 films. If this concept is extended to porous thin films, the expected change of the interference color upon adsorption or desorption of a volatile species suggests a novel concept for chemical sensing or detection. Sensing in porous films has already been described in several publications,[4−8] also in combination with Bragg stacks.[9−13] Whereas in previous studies the sensitivity of the porous structure was achieved by using nanoparticle-based[10] or mesoporous-based[11,12] layers, we have combined both morphologies into one platform to maximize the porosities and surface areas and thus to potentially enhance the achievable optical response. Other important aspects of porous nanoparticle-based Bragg stack designs are discussed below.

While for sensing applications pore accessibility throughout the multilayer system must be guaranteed by high porosities, a high refractive index contrast between the two layer materials needs to be maintained. In a former publication,[14] synthesis procedures for the preparation of nanoparticulate colloidal suspensions of phenyl-functionalized mesoporous silica nanoparticles were reported. These colloidal suspensions are ideal candidates for the production of highly porous homogeneous thin films with a low refractive index. For the high refractive index layer, nanoparticulate colloidal titania is a suitable material. The preparation of thin films with mesoporous nanoparticles offers several advantages over the common template-directed evaporation induced self-assembly (EISA) approach for mesoporous films or the *in situ* growth of nanocrystalline zeolite films, on substrates: (a) Thin films made of randomly oriented mesoporous nanoparticles exhibit improved diffusion properties and a highly accessible pore system.[15] (b) In contrast to mesoporous sol−gel films, which are highly sensitive to the aging conditions, it is possible to prepare stable suspensions of already extracted and characterized nanoparticles, thus assuring good reproducibility and well-characterized sorption properties. (c) The film thickness can be controlled over a wide range by varying the particle concentration or the number of coating steps. (d) The coating of sensitive substrates as

*Address correspondence to bein@lmu.de.

Received for review December 31, 2008 and accepted April 23, 2009.

Published online June 19, 2009.
10.1021/nn800911c CCC: $40.75

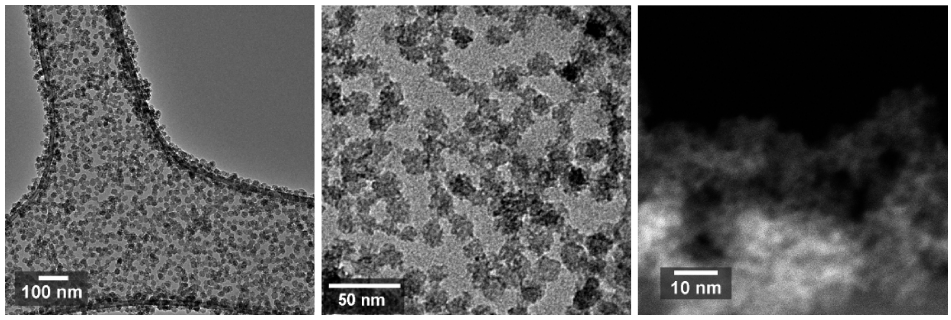

Figure 1. TEM micrographs of CMS-20 (right: HAADF-STEM, high angle annular dark field scanning transmission electron microscopy).

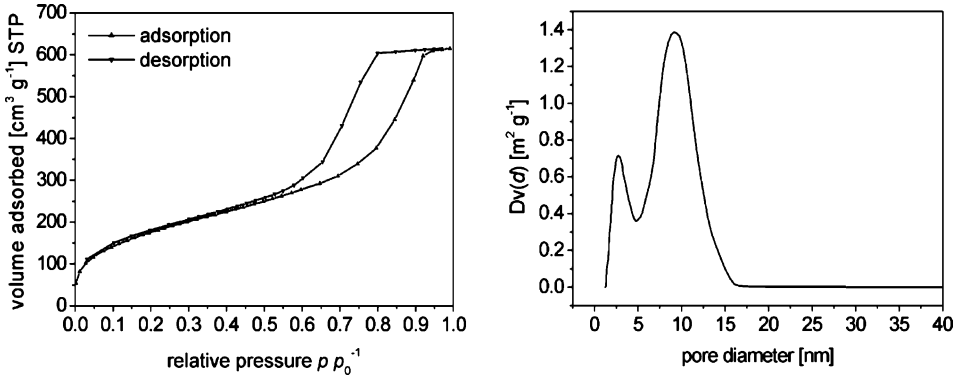

Figure 2. N_2 sorption data and pore size distribution of dried, extracted CMS-20.

well as the integration of delicate layer materials is facilitated due to the mild processing conditions. For example, intricate or high-temperature template removal procedures between the coating steps are not required. (e) The last-coated layers are located only on top of the layer structure—no soluble precursor constituents may percolate into the already deposited underlying layer structure. (f) The high external and internal surface areas of the mesoporous nanoparticles allow for purposeful functionalization by one-pot procedures or postsynthesis grafting to impart specific sensing properties to the layers. We have recently reported the preparation of related porous thin films of functionalized mesoporous silica nanoparticles.[16]

Such Bragg mirrors have numerous potential applications, such as in sensing devices, wavelength-selective tunable optical filters in a broad spectral range, and reflective coatings. By combining the tunable reflective properties of Bragg mirrors with the physicochemical properties of the constituent layers, we can probe the adsorption behavior of the Bragg mirrors as a function of the vapor pressure, that is, the optical adsorption isotherm.[10,17]

RESULTS AND DISCUSSION

Characterization of CMS-20. It was possible to synthesize colloidal suspensions of functionalized mesoporous silica nanoparticles with a very small particle size. Figure 1 shows transmission electron micrographs (TEM) of CMS-20 (colloidal mesoporous silica, 20 nm) with an average particle diameter around 20 nm. The size distribution of the discrete particles is very narrow. High-resolution images clearly show the porous nature of the functionalized particles.

In order to investigate the sorption properties of the porous nanoparticles, the ethanolic suspension was dried at 60 °C. The resulting solid was colorless and transparent, consisting of small platelets with about 1 mm diameter. Despite its dense appearance, the material has a high specific surface area of 640 $m^2 g^{-1}$, as determined from nitrogen sorption isotherms, as well as a high pore volume of 0.95 $cm^3 g^{-1}$. NLDFT equilibrium calculations based on the desorption branch resulted in a bimodal pore size distribution (Figure 2).

The first peak at 2.7 nm due to templated mesopores is in the expected range for functionalized mesoporous silica templated by hexadecyltrimethylammonium ions. The second peak around 10 nm reflects the textural porosity of the material.

Characterization of CMT-80. The formation of TiO_2 particles in the initial synthesis solution caused a slowly increasing turbidity resulting in a white viscous suspension. Subsequent washing and redispersion led to an ethanolic suspension of titanium dioxide nanoparticles (sample CMT-80, colloidal mesoporous titania, 80 nm). Peptization of the particles was achieved by addition of small amounts of water (about 0.1 g mL^{-1}). The resulting colloidal, translucent suspensions showed a narrow particle size distribution in dynamic light scattering (DLS). Figure 3 shows the mean particle size (80 nm) of the suspended titania nanoparticles in the coating suspension.

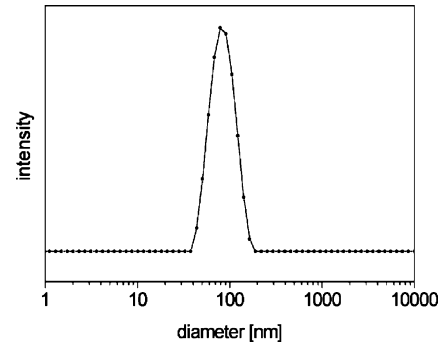

Figure 3. Particle size distribution (DLS) of CMT-80.

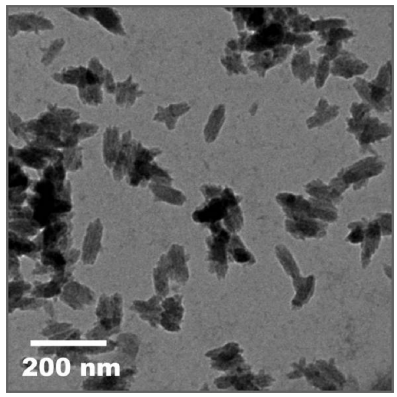

Figure 4. TEM micrograph of CMT-80.

Electron microscopy confirmed the existence of discrete particles in the nanometer range. The TiO_2 nanoparticles can be described as lath-shaped aggregates of approximately the same average length as indicated by DLS (Figure 4). X-ray diffraction of these particles indicates the presence of very small crystalline rutile domains combined with some amorphous titania phase (see Supporting Information, Figure S1), which is consistent with the high surface area and pore volume obtained from nitrogen sorption isotherms; see below.

Nitrogen sorption analysis (Figure 5) showed that the material exhibited a certain mesoporosity. CMT-80 showed a BET surface area of more than 300 $m^2\ g^{-1}$, a pore volume of 0.24 $cm^3\ g^{-1}$, and a relatively narrow pore size distribution with a diameter around 5 nm.

Due to the easy redispersibility of the washed particles and the high quality of the final ethanolic suspensions, the material can be used for the preparation of homogeneous thin films by spin-coating. Figure 6 shows an image of a silicon wafer with a thin film of titania nanoparticles. The film was prepared by spin-coating two times with a suspension containing about 3 wt % of CMT-80. The film appears very homogeneous and transparent and thus has a definite interference color. Ellipsometric measurements resulted in a film thickness of 107 nm.

In order to realize the desired film thickness as described in the following, the suspensions were diluted until the ellipsometric analysis (Figure 7) resulted in a 102 nm thin film of CMS-20 and a 40 nm thin film of CMT-80.

Bragg Stacks: Preparation and Optical Properties. The colloidal suspensions of mesoporous nanoparticles CMS-20 and CMT-80, described above, were used for the stepwise deposition of multilayer thin films on silicon wafers in order to examine the thickness, optical properties, and homogeneity of the resulting stacks (sample BS-1). After each coating step, the sample was analyzed with ellipsometry. Once the data were fitted, optical properties of these layers were not changed in the following data analysis. After the last layer was deposited, unrestricted fitting of all previous layers did only slightly improve the quality of the fit. This indicates that the previous films are not changing significantly upon heating and further deposition steps. The final homogeneous

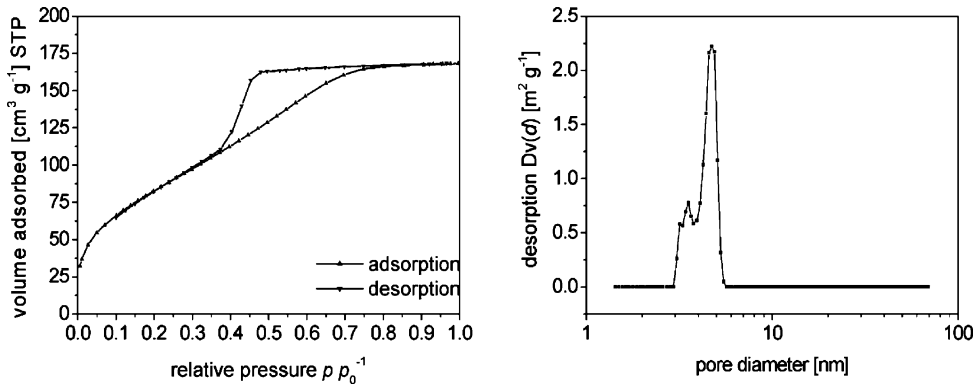

Figure 5. N_2 sorption data and pore size distribution of CMT-80.

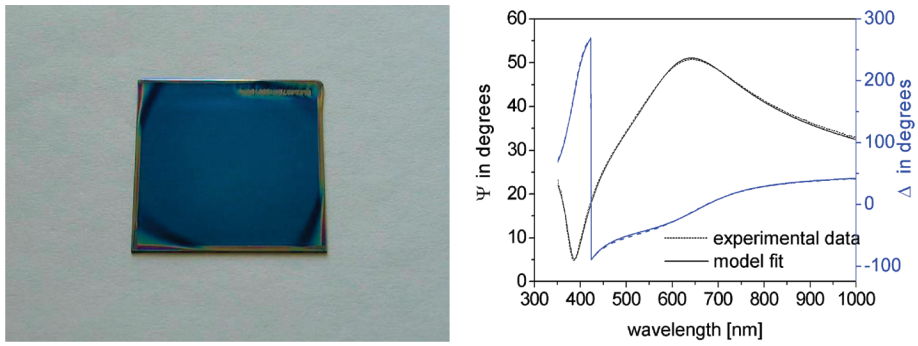

Figure 6. Thin film of CMT-80 (107 nm) on a silicon wafer and ellipsometric data.

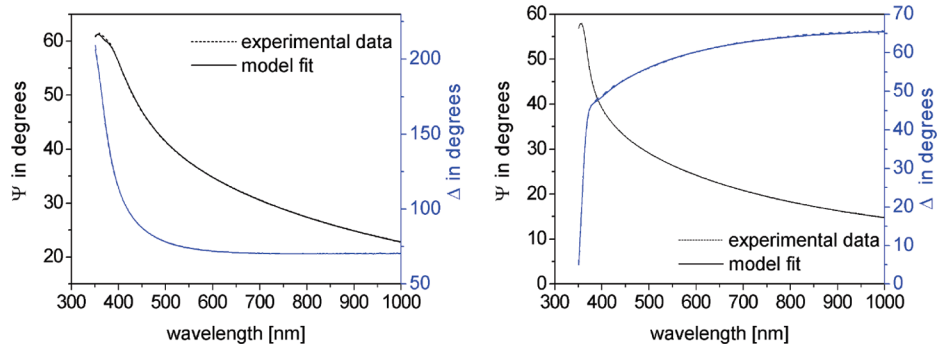

Figure 7. Ellipsometric data of a 102 nm thin film of CMS-20 (left) and a 40 nm thin film of CMT-80 (right).

film (BS-1) appeared golden. Figure 8a shows the ellipsometric data for a multilayer stack of four thin films consisting of functionalized mesoporous silica nanoparticles. The layers are alternated with mesoporous thin films of titania nanoparticles.

The data for the theoretical model stack fit the experimental data very well. The thickness of the individual layers is reproducible and varies only in a narrow range (*e.g.*, 135 ± 8 nm in the case of CMS-20). This ensures a narrow bandwidth in reflection and transmission. Table 1 shows the composition of the multilayer stack.

In the model stack shown above, the phenyl-functionalized porous silica as well as the porous titania layers are fitted using the Cauchy dispersion model for dielectric materials. Cauchy 1 represents the silica material, and Cauchy 2 stands for the titania layer. Due to the inherent porosity of both materials, the resulting refractive indices are significantly lower than for the bulk materials (n_D = 1.27 and 1.72, compared to 1.46 for glass and 2.61 for rutile, respectively). The Bragg stack structure derived from the ellipsometric data was confirmed with scanning electron microscopy. Figure 9a shows side-view micrographs of the Bragg stack BS-1. The dark layer represents the SiO_2 layers, which alternate with light TiO_2 layers. Thus, the depth profile obtained with ellipsometry is in good accordance with the SEM results (Figure 9b). On the SEM profile of Figure 9b, we have also overlaid the thickness profile obtained from the ellipsometric data (in red). From this correlation, we can deduce that the sequence of layers, their position in the film, and the overall thickness all fit well with the ellipsometric data. However, we note that the thickness of the individual titania layers in the SEM image seems to be greater than that of the silica layers. We attribute this to the fact that the titania layer is made from fairly large oblong particles that can partially interpenetrate with the silica layers made of much

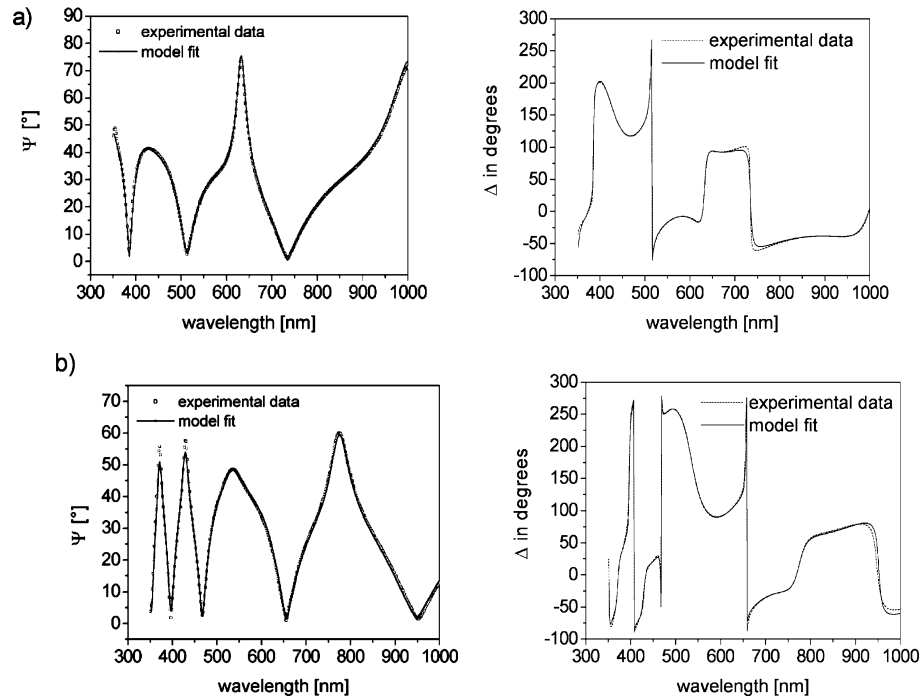

Figure 8. Experimental ellipsometry data and model fit for Bragg stack BS-1 at 75° in (a) nitrogen atmosphere and (b) toluene vapor.

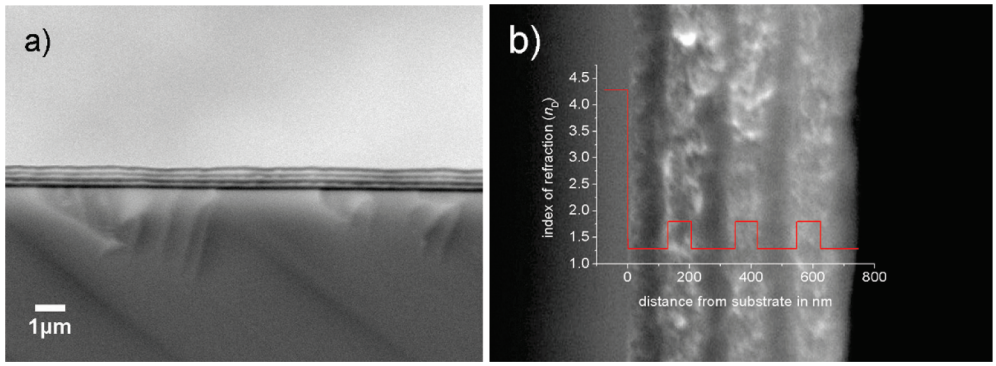

Figure 9. SEM pictures (side view) and a depth profile (ellipsometry) of Bragg stack BS-1.

smaller (20 nm) spherical silica particles. On average, however, the films are well-defined in their multilayer stack dimensions and in the resulting optical properties. The near perfect ellipsometric fits based on the simple multilayer model described above confirm the good optical definition of the films.

When exposed to a vapor of toluene close to saturation ($pp_0^{-1} = 0.86$), the color of the Bragg mirror immediately changes from yellow to red because the optical thickness of the individual layers increases due to adsorption of toluene into the pores. This change of the optical properties can be also observed in the reflectance spectra of BS-1 at an angle of 75° in a flow of dry nitrogen (solid line) and of toluene-enriched nitrogen (dotted line) in Figure 10.

Spectroscopic ellipsometry allows us to correlate the pore filling with the increase of the refractive index of the individual layers. The pronounced change due to sorption of toluene can be seen when comparing Figure 8a and Figure 8b. The exchange of the gaseous nitrogen by liquid toluene inside the porous multilayer stack significantly influences the refractive index of the individual films.

Fitting of the new experimental data after vapor sorption is achieved by simply increasing the refractive index of the layers at constant film thickness. Thus, the n_D value for the silica layers increases from 1.27 to 1.48, and the one for the titania layers from 1.72 to 1.93. Figure 8b shows the experimental data and the model fit of BS-1 in gaseous toluene with modified optical properties. The good correlation confirms the theory of filled pores.

The total porosity is calculated with ellipsometric porosimetry using the Lorentz−Lorenz equation. It is based on the Clausius−Mossotti equation, which describes the relation between the macroscopic measurable relative dielectric constant and the electric polarizability α. The adsorption of volatile species in the film changes its refractive index. When the refractive index of the filled and empty porous substrate is known, one can determine the porosity of the material without knowing the refractive index of the dense material (see

TABLE 1. Layer Thicknesses of the Sample BS-1 Determined with Ellipsometry

number of layer	layer description	thickness [nm]
8	Cauchy 1	127
7	Cauchy 2	74
6	Cauchy 1	129
5	Cauchy 2	76
4	Cauchy 1	135
3	Cauchy 2	73
2	Cauchy 1	143
1	silicon dioxide	2
0	silicon	10^6

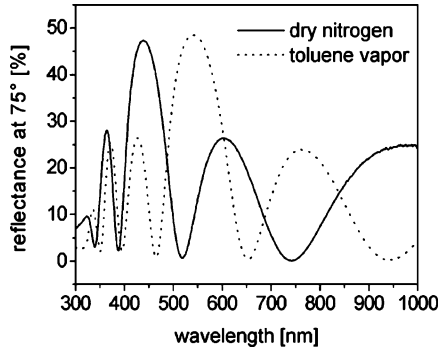

Figure 10. Reflectance spectra of BS-1 in dry nitrogen (solid line) and toluene vapor (dotted line).

TABLE 2. Refractive Indices and Porosities of the Layers in BS-1 Determined with Ellipsometric Porosimetry

layer description	n_D in dry nitrogen	n_D in toluene vapor	n_D toluene	porosity (%)
Cauchy2 (titania)	1.718	1.925	1.496	27.7
Cauchy1 (silica)	1.266	1.476	1.496	39.3

TABLE 3. Desired and Actual Layer Thicknesses and Optical Properties of the Bragg Stack BS-2

	modified silica	titania
reflected color	green	UV
selected wavelength range	500−550 nm	<350 nm
optical thickness	~130 nm	<90 nm
refractive index of filled layer (325 nm)	—	1.93
refractive index of filled layer (525 nm)	1.28	—
theoretical film thickness	~100 nm	<47 nm
realized film thickness	102 nm	40 nm

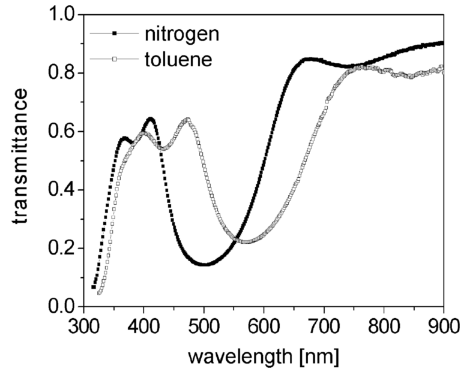

Figure 11. Wavelength shift in transmittance spectra due to adsorption of toluene vapor in Bragg stack BS-2 (samples in a quartz cuvette).

Supporting Information for more details). The resulting values are listed in Table 2.

Knowing the optical properties of the constituent materials, one can predict the optical properties of Bragg reflectors with different thicknesses for wavelength-selective coatings. The optical thickness (OT) of the layers is adjusted to one-fourth of the desired wavelength (OT = λ/4). Depending on the refractive index of the material, the physical thickness of the film is calculated (OT n^{-1}). If the Bragg mirror is supposed to reflect the green part of the light (500−550 nm), the optical thickness of the layers should be about 130 nm. In order to observe a color change depending mainly on the low refractive and modifiable SiO_2 layer, the titania layer was chosen thin enough to realize an optical thickness (OT) outside the visible part of the light (OT < 100 nm), even in the filled state (refractive index of the toluene-filled layer at 350 nm: 1.93). Table 3 shows the desired and realized optical properties of the prepared individual layers of a green reflecting Bragg stack (BS-2).

For the preparation of this stack, the concentration of the colloidal suspensions and the spinning rate of the spin-coater were adjusted in order to realize the formation of thin films with the above-mentioned thickness for reflecting green light. Single layers of the films were deposited on silicon wafers in order to examine their thickness, before the preparation of the stack was performed on a glass plate.

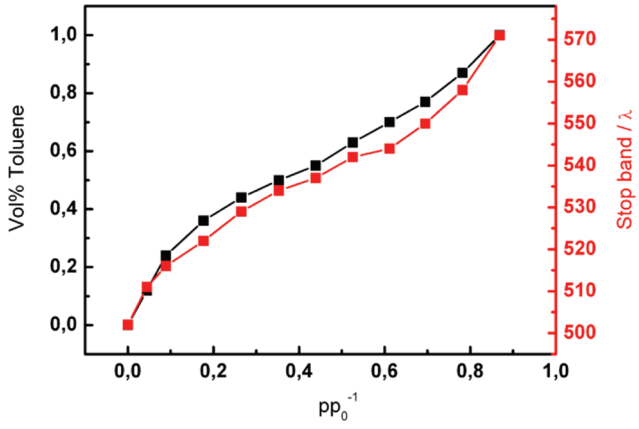

Figure 12. Red line: Wavelength shift of transmitted light in BS-2 at different relative pressures of toluene (0° incident angle). Black line: Simulation of the corresponding volume percentage of toluene pore filling. For the linear-scale display, the starting points at 0% loading and the end of the isotherms at full pore filling are overlaid.

The desired reflected wavelength of the Bragg mirror (maximum ~ 525 nm) was confirmed with optical transmission measurements. Figure 11 shows the transmittance spectrum of stack BS-2. The transmittance minimum is at 500 nm. The Table of Contents figure shows the color of the transmitted and reflected light of the Bragg stack BS-2 in air. The coated transparent glass plate (held perpendicular) is illuminated from the left side with sunlight. The transmitted and reflected light falling onto the table is complementary. Due to the illumination angle, the light is shifted to shorter wavelengths (Bragg's law).

Bragg Stack: Vapor Sorption. The stack was placed in a quartz cuvette with gas inlet and outlet in order to follow the change in the transmittance color of the Bragg reflector after adsorption of vapor. In an atmosphere of toluene (pp_0^{-1} = 0.86), the adsorption of toluene increases the optical thickness of the adsorbing layer and thus drastically changes the reflected as well as the transmitted wavelength. This change can be clearly seen in the transmission spectrum (Figure 11). The transmission minimum (reflection maximum) changes from about 500 (blue) to 570 nm (yellow). This change happens within seconds when the film is exposed to the toluene vapor.

The optical shifts observed at different relative pressures of toluene are plotted in Figure 12. By taking advantage of the optical parameters obtained by ellipsometry and ellipsometric porosimetry, transmission spectra mapping the incremental increase of toluene pore filling could be simulated based on an effective medium approach considering partially air- and toluene-filled pores. This approach enables a direct correlation between the fractional pore filling and the observed optical shifts, thus furnishing an optically encoded adsorption isotherm (or optical isotherm) as displayed in Figure 12.

The good correlation between the shapes of both curves highlights the direct translation of the relative pore filling into the observed optical shifts. Accordingly, both optical and adsorption isotherms exhibit similar features with both curves partially resembling a type IV isotherm, which is typical for mesoporous materials. After a relatively steep increase, they pass nearly a plateau at a relative pressure of about 0.53 before the slope increases again at about 0.70. The adsorption at higher relative pressures is attributed to filling of textural porosity caused by packing of the individual particles in the film. We note that in the analysis of the experimental data we have assumed a proportional increase in the relative percentage of solvent filling for both layer types (see Methods). While a more detailed

analysis of the complex adsorption in mixed porous layers (see, *e.g.*, ref 11) must await further work, the close match of the shape of the two isotherms suggests that this simplified model provides a good representation of the adsorption behavior.

CONCLUSIONS

In summary, wavelength-specific Bragg mirrors could be prepared by a reproducible spin-coating approach from colloidal suspensions of mesoporous nanoparticles. These Bragg reflectors show sensitivity toward specific relative pressures of organic vapors such as toluene. The ability to create colloidal suspensions of various porous nanoparticles opens a wide field of possible functional Bragg mirrors. For example, the nature of the porous surface and thus the sorption properties may be varied by grafting different organic groups, thus offering different interactions with the adsorptives (or analytes) of interest. The sensitive layer can also be replaced by other porous materials, such as zeolites. Finally, the thickness of the individual layers can be tuned in order to obtain reflectance or transmittance minima or maxima at a desired wavelength, even in the UV or IR region.

METHODS

The colloidal suspensions of low refractive index material (CMS-20, porous SiO_2 nanoparticles) and high refractive index material (CMT-80, TiO_2 nanoparticles) were used for the preparation of thin films. All chemicals were purchased from Sigma-Aldrich with reagent grade (98% or higher) and used without further purification. The water was deionized.

CMS-20: The synthesis was carried out in a 100 mL glass test tube (diameter = 2.5 cm). A solution of 2.00 g of aqueous solution of cetyltrimethylammonium chloride (25 wt %), 18.00 g of deionized water, and 0.08 g of triethanolamine (TEAH) was heated to 60 °C under stirring. A mixture of 1.56 g of tetraethylorthosilicate (TEOS) and 0.18 g of phenyltriethoxysilane (PTES) was added and stirred for 1 h. The vessel was kept open in order to evaporate parts of the ethanol that were formed during the condensation. Extraction: The following solutions were prepared for the extraction of the template. **E1**: 50 g of concentrated hydrochloric acid (37% HCl) in 500 mL of ethanol. **E2**: 10 g of ammonium nitrate in 500 mL of ethanol. The resulting colloidal suspension was flocculated with 20 mL of **E1**, and the cloudy precipitate was centrifuged for 5 min at 40 000*g* (RCF). After decanting, the sediment was redispersed through vigorous stirring in 20 mL of **E2**. The clear suspension was treated for 10 min in an ultrasonic bath. After flocculating with 20 mL of deionized water, the precipitate was again centrifuged, the sediment was redispersed in 20 mL of **E1** and again sonicated. After flocculation with 20 mL of deionized water and centrifugation, the sediment can be redispersed in ethanol, leading to a suspension of colloidal mesoporous silica (CMS) with approximately 5 wt % solid content.

CMT-80: The amount of 5.52 g of concentrated hydrochloric acid (37%) was added to a solution of 11.36 g of tetraisopropylorthotitanate and 36.80 g of EtOH. The amount of 8.76 g of deionized H_2O was added, and the clear solution was refluxed under stirring for 6 h, while slowly forming a white suspension. The suspension was diluted with 20 mL of EtOH and peptized with 2 mL of water before it was centrifuged for 5 min at 40 000*g* (RCF) in order to remove big agglomerates. The supernatant suspension was flocculated with 20 g of hydrochloric acid, and after centrifugation, the sediment was redispersed in a mixture of 20 mL of EtOH and 2 g of deionized H_2O. This washing procedure was repeated twice.

Film Preparation: The homogeneous colloidal suspensions contained between 2 and 5 wt % solid nanoparticulate material. In order to remove potential inhomogeneities, the coating suspensions were filtered through 0.2 μm syringe filters prior to deposition. The thin films were deposited on polished silicon wafers or glass plates by spin-coating using a Laurell WS-400B-6NPP-Lite-AS. All substrates were precleaned with ethanol for 5 s under spinning at 3000 rpm. The film thickness was adjusted by diluting the colloidal suspensions with absolute ethanol, by variation of the spinning rate between 3000 and 5000 rpm, or by multistep coatings. After each deposition, the film was annealed for 10 s in a flow of hot air (heat gun, ~300 °C) and cooled to room temperature before measurements were performed and the next layer was added.

Film Characterization: SEM micrographs were recorded with a JEOL JSM-6500F scanning electron microscope (SEM) equipped with an Oxford EDX analysis system. Ellipsometry measurements were performed with a Woollam M2000D at an angle of 75° in the spectral range of 190−1000 nm. The data were fitted in the range between 350 and 1000 nm using a Cauchy-type material as model layer. Transmittance and reflectance measurements were recorded with the same ellipsometer using *p*-polarized light at 75 or 0°, depending on the sample and the experimental setup. In order to record the shift of the transmitted (angle = 0°) wavelength due to vapor sorption, the films were placed into a quartz cuvette with gas in- and outlet. The recording of isotherms (at 22 °C) was performed using a homemade Labview-controlled gas mixer. Digital mass flow controllers (W-101A-110-P, F-201C, Bronkhorst High-Tech) ensured the accurate dosing of the carrier gas nitrogen and the liquid analyte, which was vaporized in a controlled evaporation and mixing element (W-101A, Bronkhorst High-Tech). Partial pressures (p) were calculated using the van der Waals equation. The relative pressure pp_0^{-1} relates to the saturation pressure p_0. Simulations of the optical spectra were carried out using the program WinCPC (by Georg von Freymann, Karlsruhe) which furnishes analytically correct solutions of the 1D scalar-wave equation using the transfer matrix formalism.[18] Spectra were simulated based on the data (Cauchy models for completely N_2- and toluene-filled pores, layer thicknesses, and porosities; see Tables 2 and 3) obtained by ellipsometry and ellipsometric porosimetry. The data were fitted to the experimental transmission spectra measured at relative pressures of toluene where $0 < pp_0^{-1} < 0.86$. The starting and final thicknesses (after adsorption) of the SiO_2 and TiO_2 layers used in the simulations were determined by adapting the simulated spectra to the ellipsometric fits (nk-files based on a Cauchy model) at $pp_0^{-1} = 0$ and 0.86, respectively, while including a slight solvent swelling of the layers by less than 2 nm. Throughout the simulations, the composition of each layer was varied in steps from the empty state (in vol %) of 72.3% TiO_2 + 27.7% air + 0% toluene/60.7% SiO_2 + 39.3% air + 0% toluene to the completely filled state 72.3% TiO_2 + 0% air + 27.7% toluene/60.7% SiO_2 + 0% air + 39.3% toluene, assuming a proportional increase in the relative percentage of solvent filling for both layer types.

Acknowledgment. G.A.O. is Government of Canada Research Chair in Materials Chemistry. Funding granted by NSERC, the University of Toronto, and the Alexander von Humboldt Foundation (Feodor−Lynen postdoc scholarship for B.V.L.), as well as Deutsche Forschungsgemeinschaft (SFB 486, NIM Cluster) is gratefully acknowledged. We thank Wacker Siltronic AG for the donation of silicon wafers, and S. Schmidt and M. Döblinger for the recording of electron micrographs.

Supporting Information Available: Theory of ellipsometric porosimetry, powder X-ray diffractogram of sample CMT-80. This material is available free of charge *via* the Internet at http://pubs.acs.org.

REFERENCES AND NOTES

1. Chichibu, S. F.; Ohmori, T.; Shibata, N.; Koyama, T. Dielectric SiO_2/ZrO_2 Distributed Bragg Reflectors for ZnO Microcavities Prepared by the Reactive Helicon-Wave-Excited-Plasma Sputtering Method. *Appl. Phys. Lett.* **2006**, *88*, 161914/1.
2. Bardosova, M.; Pemble, M. E.; Povey, I. M.; Tredgold, R. H.; Whitehead, D. E. Enhanced Bragg Reflections from Size-Matched Heterostructure Photonic Crystal Thin Films Prepared by the Langmuir−Blodgett Method. *Appl. Phys. Lett.* **2006**, *89*, 093116/1.
3. Parker, A. R.; McKenzie, D. R.; Large, M. C. J. Multilayer Reflectors in Animals Using Green and Gold Beetles as Contrasting Examples. *J. Exp. Biol.* **1998**, *201*, 1307–1313.
4. Palaniappan, A.; Su, X.; Tay, F. Functionalized Mesoporous Silica Films for Gas Sensing Applications. *J. Electroceram.* **2006**, *16*, 503–505.
5. Nicole, L.; Boissiere, C.; Grosso, D.; Hesemann, P.; Moreau, J.; Sanchez, C. Advanced Selective Optical Sensors Based on Periodically Organized Mesoporous Hybrid Silica Thin Films. *Chem. Commun.* **2004**, 2312–2313.
6. Yuliarto, B.; Zhou, H.; Yamada, T.; Honma, I.; Katsumura, Y.; Ichihara, M. Effect of Tin Addition on Mesoporous Silica Thin Film and Its Application for Surface Photovoltage NO_2 Gas Sensor. *Anal. Chem.* **2004**, *76*, 6719–6726.
7. Bearzotti, A.; Mio Bertolo, J.; Innocenzi, P.; Falcaro, P.; Traversa, E. Relative Humidity and Alcohol Sensors Based on Mesoporous Silica Thin Films Synthesised From Block Copolymers. *Sens. Actuators, B* **2003**, *B95*, 107–110.
8. Wirnsberger, G.; Scott, B. J.; Stucky, G. D. pH Sensing with Mesoporous Thin Films. *Chem. Commun.* **2001**, 119–120.
9. Choi, S. Y.; Mamak, M.; von Freymann, G.; Chopra, N.; Ozin, G. A. Mesoporous Bragg Stack Color Tunable Sensors. *Nano Lett.* **2006**, *6*, 2456–2461.
10. Colodrero, S.; Ocana, M.; Gonzalez-Elipe, A. R.; Miguez, H. Response of Nanoparticle-Based One-Dimensional Photonic Crystals to Ambient Vapor Pressure. *Langmuir* **2008**, *24*, 9135–9139.
11. Fuertes, M. C.; Colodrero, S.; Lozano, G.; Gonzalez-Felipe, A. R.; Grosso, D.; Boissiere, C.; Sanchez, C.; de Soler-Illia, G. J. A. A.; Miguez, H. Sorption Properties of Mesoporous Multilayer Thin Films. *J. Phys. Chem. C* **2008**, *112*, 3157–3163.
12. Fuertes, M. C.; López-Alcaraz, F. J.; Marchi, M. C.; Troiani, H. E.; Luca, V.; Míguez, H.; Soler-Illia, G. J. A. A. Photonic Crystals from Ordered Mesoporous Thin-Film Functional Building Blocks. *Adv. Funct. Mater.* **2007**, *17*, 1247–1254.
13. Lotsch, B. V.; Ozin, G. A. Photonic Clays: A New Family of Functional 1D Photonic Crystals. *ACS Nano* **2008**, *2*, 2065–2074.
14. Kobler, J.; Möller, K.; Bein, T. Colloidal Suspensions of Functionalized Mesoporous Silica Nanoparticles. *ACS Nano* **2008**, *2*, 791–799.
15. Lee, U. H.; Kim, M.-H.; Kwon, Y.-U. Mesoporous Thin Films with Accessible Pores from Surfaces. *Bull. Korean Chem. Soc.* **2006**, *27*, 808–816.
16. Kobler, J.; Bein, T. Porous Thin Films of Functionalized Mesoporous Silica Nanoparticles. *ACS Nano* **2008**, *2*, 2324–2330.
17. Salem, M. S.; Sailor, M. J.; Harraz, F. A.; Sakka, T.; Ogata, Y. H. Sensing of Chemical Vapor Using a Porous Multilayer Prepared from Lightly Doped Silicon. *Phys. Status Solidi C* **2007**, *4*, 2073–2077.
18. Born, M.; Wolf, E. *Principles of Optics*; Pergamon: New York, 1964.